The Tropical Dynamical Response to Latent Heating Estimates Derived from the TRMM Precipitation Radar

COURTNEY SCHUMACHER, ROBERT A. HOUZE JR., AND IAN KRAUCUNAS

Department of Atmospheric Sciences, University of Washington, Seattle, Washington

(Manuscript received 29 January 2003, in final form 7 December 2003)

ABSTRACT

A 3-yr (1998–2000) climatology of near-surface rainfall and stratiform rain fraction observed by the Tropical Rainfall Measuring Mission (TRMM) precipitation radar (PR) was used to calculate the four-dimensional distribution of tropical latent heating on seasonal-to-annual time scales. The TRMM-derived latent heating was then used to force an idealized primitive equation model using an initial value approach in order to obtain the quasi-steady-state, nonlinear, zonally asymmetric atmospheric response to precipitating tropical cloud systems. In agreement with previous studies, an increase in stratiform rain fraction elevates circulation centers and strengthens the upper-level response. Furthermore, horizontal variations in the vertical heating profile implied by the PR stratiform rain fraction pattern lead to circulation anomalies of varying height and vertical extent that are not present when the model is forced with a vertically uniform heating field. During El Niño, the trans-Pacific gradient in stratiform rain fraction that is normally present becomes more pronounced and the model response becomes even more sensitive to the horizontal variability of the latent heating vertical structure. When the heating field is modified to take into account the effects of nonprecipitating cumulus and cloud radiative forcing within the regions of tropical precipitating cloud systems, the overall pattern of the model response to the TRMM-derived latent heating is reinforced, as is the model's sensitivity to the variability in the latent heating vertical structure.

1. Introduction

The large-scale dynamical response to variations in the vertical heating profile associated with tropical precipitating systems has generally received less attention than the response to horizontal variations in convective activity, even though the generation of potential vorticity in the Tropics is directly proportional to the local vertical gradient in the heating profile (Haynes and McIntyre 1987; Mapes and Houze 1995). The studies that have investigated how the vertical structure of tropical heating influence the dynamical response (Geisler 1981; Hartmann et al. 1984; DeMaria 1985; Sui and Lau 1989; Wu et al. 2000; Chiang et al. 2001) all assume geographically uniform vertical heating profiles; however, vertical heating profiles of precipitating cloud systems have been observed to vary over space and time across the Tropics (e.g., Thompson et al. 1979; Frank and McBride 1989).

Attempts to link horizontal variations in the vertical structure of tropical heating in precipitating cloud systems to specific large-scale circulation features have been hampered by the lack of high-resolution data over large time and space scales. Condensational heating generated by general circulation models is strongly dependent on the model parameterizations and is not always consistent with observations (Nigam et al. 2000; Lin et al. 2004). The horizontal and vertical distribution of total diabatic heating can be calculated as a residual using the equations of motion and observed winds and temperatures (e.g., Valdes and Hoskins 1989; Nigam 1994; Wang and Ting 1999). However, the residual heating estimates represent the total apparent heat source so it is difficult to separate the latent, sensible, and radiative heating components, and the accuracy of the residual method is uncertain over the Tropics because of sparse data availability (White and Saha 1995; Waliser et al. 1999; Newman et al. 2000; Kistler et al. 2001). Passive microwave instruments on board satellites supply Tropics-wide observations of precipitating systems that can be used to derive the horizontal and vertical tropical latent heating field (Tao et al. 1990; Olson et al. 1999). However, passive microwave radiometers provide limited information on the vertical distribution of hydrometeor types making estimates of the vertical structure of latent heating uncertain.

One of the primary goals of the Tropical Rainfall Measuring Mission (TRMM) was to determine the four-dimensional distribution of latent heating in the Tropics in order to better understand global climate (Simpson

Corresponding author address: Professor Courtney Schumacher, Department of Atmospheric Sciences, Texas A&M University, 3150 TAMU, College Station, TX 77843-3150.
E-mail: courtney@ariel.met.tamu.edu

et al. 1988). The novel instrument installed on board the TRMM satellite to accomplish this goal was the precipitation radar (PR). The precipitation field detected by the PR provides the column-integrated latent heating over the entire Tropics, and the detailed structure of the radar echoes allows the convective and stratiform components of the rain to be identified (Schumacher and Houze 2003a). Houze (1982, 1989) demonstrated that the relative proportions of convective and stratiform rain amounts can be used to infer the vertical structure of latent heating in tropical precipitating systems. Higher fractions of stratiform rainfall are associated with an upward shift in the level of maximum heating and an increase in the vertical heating gradient in the upper troposphere. Using observations of surface rainfall separated into convective and stratiform components, the TRMM PR is thus able to provide an estimate of the horizontal and vertical structure of latent heating across the Tropics (see also Tao et al. 2001).

The objective of this study is to determine whether latent heating estimates derived from the TRMM PR can be used to gain new insights into the large-scale circulation of the Tropics, especially with respect to horizontal and temporal variability in the percent of rain that is stratiform. Specifically, we use TRMM PR precipitation and stratiform rain fraction measurements to estimate the mean three-dimensional heating distribution during different subsets of the 1998–2000 TRMM study period, and then use an idealized version of the Community Climate Model, version 3 (CCM3), to obtain the zonally asymmetric dynamical response associated with each heating estimate. Integrations were also performed using latent heating estimates calculated with geographically uniform stratiform rain fractions and with additional diabatic heating terms included in the vertical heating profiles.

2. TRMM PR observations

For the 3 years under investigation in this study (1998–2000), the TRMM satellite operated at an altitude of 350 km, which gave the PR a swath width of 215 km and a horizontal footprint of 4.3 km at nadir. The TRMM satellite has an orbital domain extending from 35°N–35°S and has a precessing orbit so that it samples the full diurnal cycle. The PR operates at K_u band (2.17-cm wavelength) with a sensitivity ~17 dBZ (which corresponds to a precipitation rate of approximately 0.4 mm h^{-1}) and a vertical resolution of 250 m. Further details on the PR and the TRMM satellite can be found in Kummerow et al. (1998) and Kozu et al. (2001).

The radar echo observed by the PR is subdivided into convective and stratiform elements in TRMM product 2A23 (TRMM products are available online at http://daac.gsfc.nasa.gov).[1] The convective classification refers to regions of young, active convection, where stronger vertical air motions predominate, and precipitation particles increase in mass through coalescence and/or riming. The stratiform classification represents regions of less active convection, where weaker vertical air motions predominate, and precipitation particles increase in mass primarily through vapor deposition (Houze 1993). Extensive stratus and stratocumulus cloud decks that have tops well below the 0°C level and occasionally produce drizzle or light rain are also commonly considered stratiform. However, the 17-dBZ sensitivity threshold of the TRMM PR guarantees that most, if not all, of this stratiform rain is excluded from this study.

Radar reflectivity observations cannot always be unambiguously separated into regions of convective and stratiform precipitation, which occasionally leads to a third ''transition'' or ''intermediary'' classification. However, Mapes and Houze (1995) showed that only two modes account for most of the large-scale atmospheric response to convection and that these modes correspond to the divergence signatures in convective and stratiform precipitation regions. The transition/intermediary classification therefore represents an inability to definitively separate precipitation into convective and stratiform components using the radar reflectivity field, rather than a physically distinct phenomenon. Houze (1997) argues that the intermediary echo in reflectivity is more closely related to the stratiform region in terms of microphysical and dynamical processes; therefore, we separate tropical precipitation into only two categories: that of young, vigorous convection (convective) and that of older, weaker convection (transition/intermediary and stratiform).

The convective–stratiform separation algorithm used in TRMM product 2A23 (Awaka et al. 1997) determines whether the echo is convective or stratiform by examining the vertical profile of reflectivity (from which the bright band, echo top height, and maximum reflectivity in the vertical profile are identified) and the horizontal variability of the echo. The horizontal variability criterion follows Steiner et al. (1995). Within the 2A23 algorithm, pixels of radar echo are designated as ''shallow, isolated'' whenever the echo top is lower than the climatological 0°C level by 1.5 km and the pixel is isolated from other rainy areas. We consider these pixels to be a subset of the convective category (see Schumacher and Houze 2003b).

To determine the rain amounts in the convective and stratiform categories, we use the near-surface[2] PR reflectivity field from TRMM product 2A25 (Iguchi et al. 2000). Following Schumacher and Houze (2003a), reflectivity from the orbital data is placed into 2.5° bins for each month and converted to rain rate using the

[1] This study is based on version 5 data products.

[2] The PR cannot detect rain directly above the ground because of contamination from surface return. The lowest level free from surface clutter is ~1 km above the surface at nadir and ~2 km above the surface at the antenna scan edge.

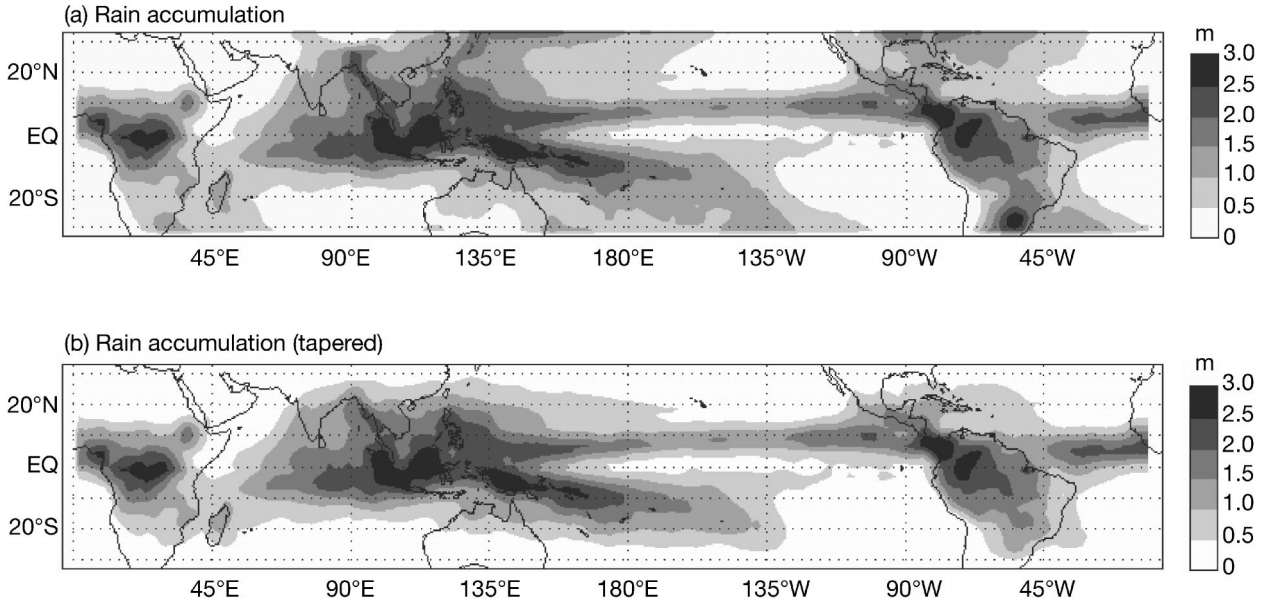

FIG. 1. (a) Precipitation radar 2.5° annually averaged rain accumulation from 1998–2000 based on TRMM product 2A25 (version 5) near-surface reflectivities converted to rain rate with the version 5 initial convective and stratiform *Z–R* relations. (b) Same as (a) except that the precipitation has been multiplied by a scaling factor that decreases linearly from a value of 1 at 20°N and 20°S to 0 at 35°N and 35°S in order to isolate the tropical heating.

TRMM version 5 convective and stratiform near-surface initial reflectivity–rain rate relations. The average convective and stratiform rain rate in each grid box is then multiplied by the probability of rain of each rain type to obtain the convective and stratiform rain amounts.

The total annually averaged rain accumulation observed by the TRMM PR during 1998–2000 is depicted in Fig. 1a. As observed in other rain climatologies, precipitation amounts are highest (>2.5 m yr^{-1}) over central Africa, the Maritime Continent, and Central and South America, and well-defined intertropical convergence zones (ITCZ) are located in the Pacific and Atlantic Oceans between 5°–10°N. In order to focus on the latent heating associated with tropical convection and eliminate edge effects at the boundaries of the PR observational domain, the precipitation field outside of 20°N and 20°S was multiplied by a scaling factor that decreases linearly from unity at 20° latitude to zero at 35°N and 35°S. The precipitation field produced by this scaling procedure is shown in Fig. 1b. This scaling procedure was found to have little effect on the model results near the equator, and increased the stability of our model integrations by retarding the growth of baroclinic disturbances along the edge of the PR domain.

The climatological stratiform rain fraction (i.e., the percentage of total rainfall accounted for by stratiform precipitation) observed by the TRMM PR from 1998–2000 is shown in Fig. 2. The stratiform rain fraction is generally lower over land and higher over the oceans, although some ocean areas outside regions of deep convection have low stratiform rain fractions (e.g., 10°–20°S, 120°–80°W). A few regions with very low precipitation rates exhibit unrealistically high stratiform rain fractions (e.g., over northern Africa and off the coast of Baja), most likely due to sampling errors. Very high stratiform rain fractions are also observed in broad regions with low to moderate precipitation poleward of 20°N and 20°S; these features are associated with extratropical systems occasionally precipitating at these latitudes. Note that the scaling procedure used to de-

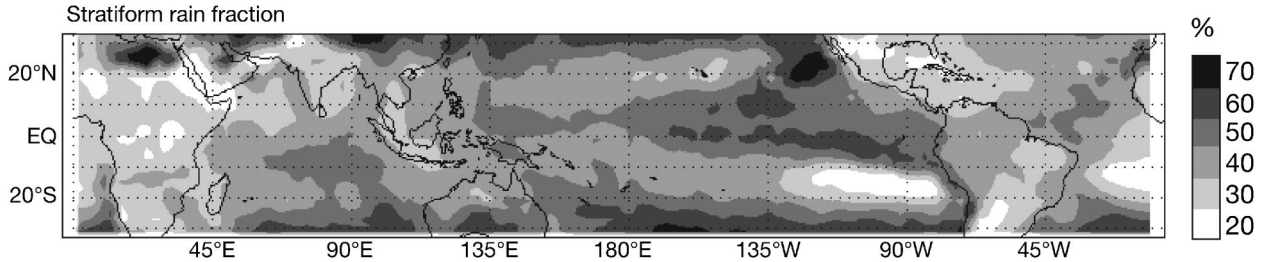

FIG. 2. Precipitation radar 2.5° average stratiform rain fraction from 1998–2000 based on TRMM product 2A23 (version 5) convective–stratiform classifications with the shallow, isolated pixels reclassified as convective.

emphasize the extratropical rain pattern (cf. Fig. 1b) minimizes the influence of these midlatitude storms on the heating estimates derived in the next section.

Perhaps the most interesting feature in the stratiform rain fraction field is a strong trans-Pacific gradient with a minimum over the Maritime Continent and a maximum in the ITCZ of the eastern-central Pacific. This near-equatorial trans-Pacific gradient, which exists throughout the seasonal cycle and becomes exaggerated during El Niño, accounts for some of the more striking results of the model calculations described in the following sections. For a more detailed discussion of the temporal and spatial variations in the PR stratiform rain fraction, see Schumacher and Houze (2003a).

3. Latent heating estimates

The total diabatic heating associated with precipitating systems can be separated into three components: latent heating and cooling associated with condensation, evaporation, and melting; radiative heating and cooling from solar and infrared absorption and emission within the cloud deck; and the vertical convergence of sensible heat flux associated with cloud-scale updrafts and downdrafts. Studies using large rawinsonde systems diagnose the atmospheric budget associated with total diabatic heating, whereas dual-Doppler studies usually diagnose divergence, which is directly related to heating from water phase changes only. Latent heating is the dominant component in the total diabatic heating, so in order to focus our attention on this component, we base our assumed heating profiles on dual-Doppler studies of mesoscale precipitation systems observed during tropical field programs (e.g., see Figs. 10–11 in Cifelli and Rutledge 1998). Thus, our profiles represent only the dominant latent heating component. Radiative heating is the next largest component of the total diabatic heating and will be addressed in section 8. Vertical eddy heat transports are ignored since they are relatively minor (Houze 1982).

To obtain the latent heating profile within each 2.5° grid box, assumed latent heating profiles associated with stratiform and convective precipitation are linearly combined based on the PR rain fraction for each precipitation type, normalized such that the area under the curve equals one, and then multiplied by the PR precipitation at each location. Thus, the three-dimensional latent heating field can be estimated for any subset of the TRMM observational period. To minimize sampling errors, this study uses seasonal-to-annual average subsets to represent the four-dimensional tropical latent heating field.

Our assumed latent heating profiles for each rain type are illustrated in Fig. 3a. The heating profile associated with deep convective rain is positive throughout the troposphere, while the stratiform profile is dominated by heating above the climatological 0°C level and cooling below. In order to use some of the height information

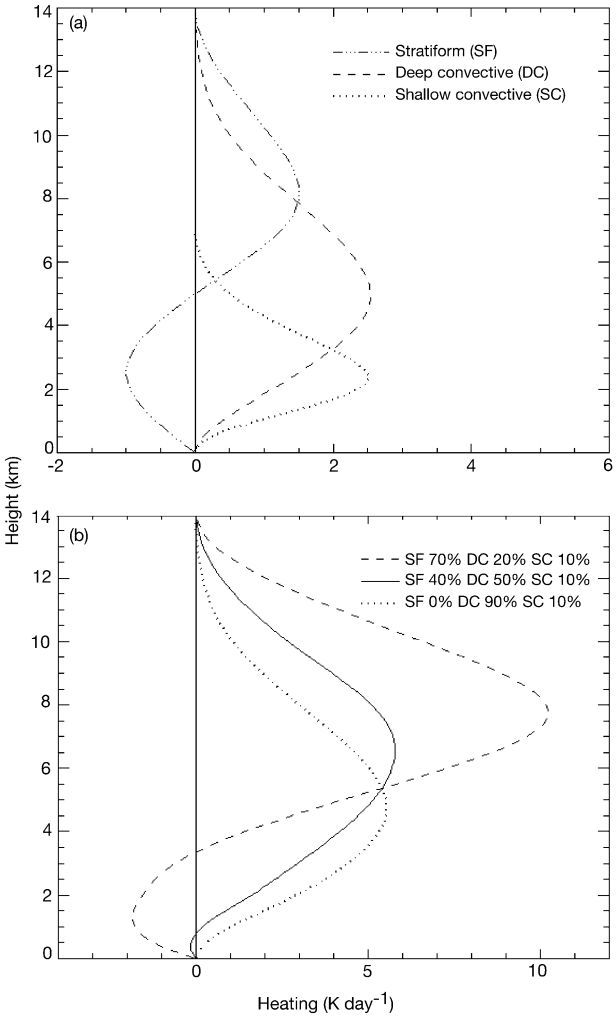

FIG. 3. Idealized stratiform, deep convective, and shallow convective latent heating profiles. The *x* axis is meant to be nondimensional until a precipitation amount is specified. (b) Total latent heating profiles for 0%, 40%, and 70% stratiform rain fractions, assuming 3.5 m yr^{-1} rain accumulation.

provided by the PR, the shallow convective classification from TRMM product 2A23 was assigned a separate latent heating profile. Since shallow convection does not represent a fundamentally different physical process from deep convection, the profile for shallow convective rain is similar to the profile for deep convective rain, except that it has been vertically compressed to represent the latent heating from low- and midlevel precipitating convective clouds. Beyond the separation of shallow and deep convection, we use fixed vertical heating profiles despite the fact that cloud heights vary somewhat in nature.

Tao et al. (2001) calculated tropical latent heating from TRMM PR observations using a method similar to ours, except that they employed a database of stratiform and convective latent heating profiles based on cloud-resolving model runs in different regions of the

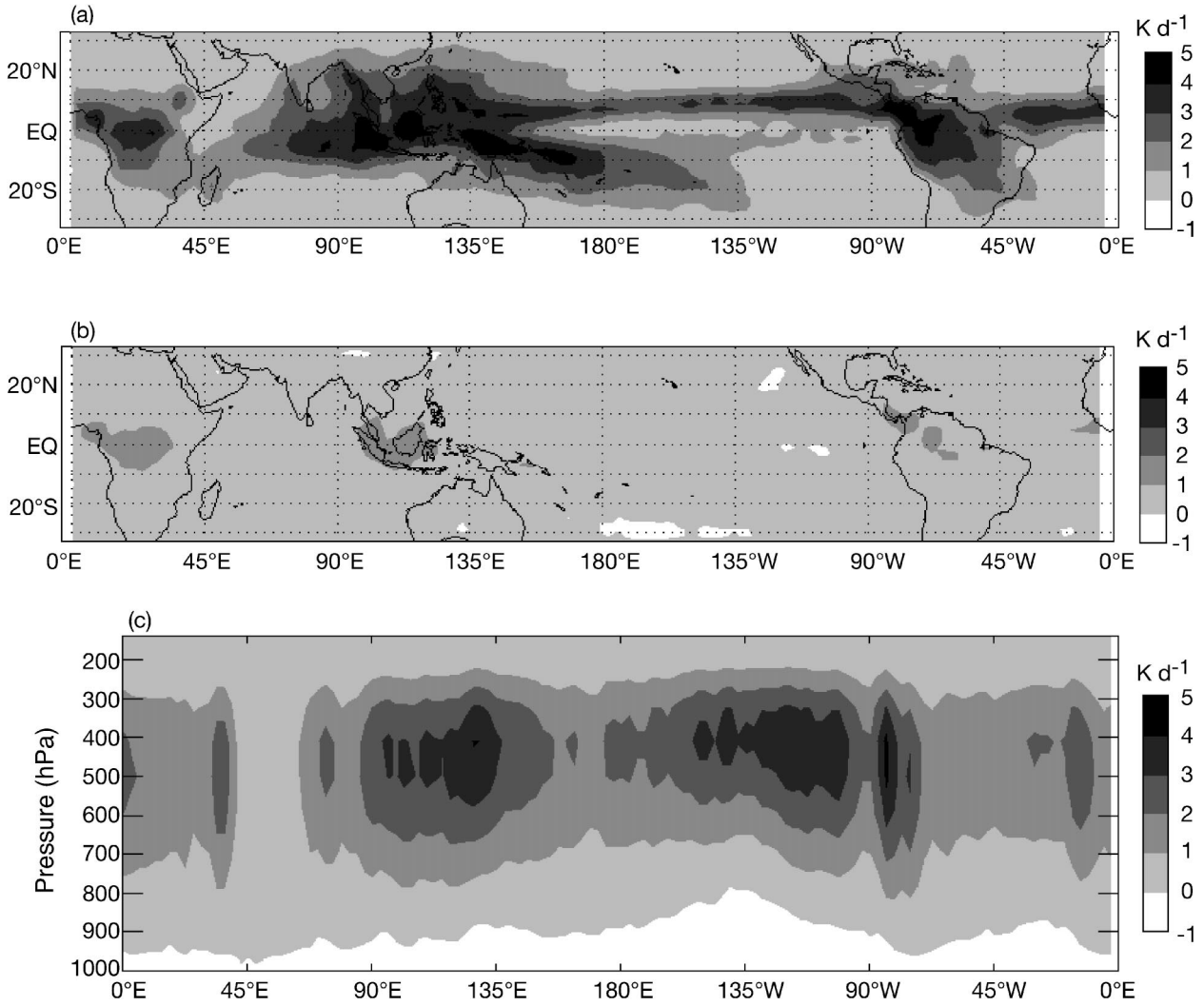

FIG. 4. Horizontal distributions of the annually averaged latent heating at (a) 7.4 km (~400 hPa) and (b) 2.2 km (~800 hPa) derived from the TRMM PR rain-type fractions and tapered rain amounts. (c) Vertical cross section of annually averaged latent heating at 10°N.

Tropics. Our assumed profiles of deep convective and stratiform latent heating are generally consistent with those calculated by Tao et al. (although Tao et al. did not include a shallow convective profile), so we would not expect the use of a larger database of latent heating profiles to alter the overall results of our study. However, Tao et al.'s results indicate some of the uncertainty associated with the profiles we have chosen.

Figure 3b illustrates the vertical profile of latent heating that would be used for a grid box with a total rainfall of 3.6 m yr^{-1}; a shallow convective rain fraction of 10%; and stratiform rain fractions of 0%, 40%, and 70%. A stratiform rain fraction of 0% (purely convective) has a heating maximum at 4.5 km, a stratiform rain fraction of 40% (which represents the Tropics-wide average) leads to a slightly stronger heating maximum at 6.5 km, and a stratiform rain fraction of 70% (the upper limit of observed climatological values) produces an even stronger heating maximum at 7.5 km, along with cooling at lower levels. In addition to raising the amplitude and height of maximum latent heat release, increasing the stratiform rain fraction produces a stronger vertical gradient of heating at upper levels.

Figure 4 illustrates the annually averaged latent heating distribution estimated from TRMM PR observations for the entire 1998–2000 study period. Figures 4a and 4b show the horizontal pattern of latent heating at 7.4 and 2.2 km, respectively, while Fig. 4c contains a vertical cross section of the annually averaged heating at 10°N. Note that the latent heating is stronger in Fig. 4a than Fig. 4b because the stratiform rain fraction is nonzero, and that the lower-level heating is concentrated over rainy regions with low stratiform rain fractions. The vertical cross section of latent heating at 10°N (Fig. 4c) further illustrates that the latent heating in regions with low stratiform rain fractions (e.g., 40°E and 85°W)

is more evenly distributed throughout the troposphere, while regions with high stratiform rain fractions (e.g., 135°W) exhibit more latent heating at upper levels.

4. Model

The atmospheric model used for this study is an idealized version of the CCM3 that has been modified to calculate the time-dependent, nonlinear, zonally asymmetric response to a fixed distribution of diabatic heating. The dynamical core of the model uses the spectral transform method in the horizontal domain with T42 resolution, which corresponds to a grid spacing of roughly 2.9° in latitude and longitude. Vertical and temporal aspects are treated using finite differences, with 18 unevenly spaced vertical levels (12 of which are located in the troposphere) and a time step of 20 min. Further discussion of the model dynamics can be found in Kiehl et al. (1998).

We force the model by adding the three-dimensional TRMM-derived latent heating distributions described in the previous section directly to the temperature tendency equation. In order to isolate the time-dependent zonally asymmetric response to the TRMM-derived heating, the boundary conditions and physical parameterizations normally employed by CCM3 were replaced with linear damping of temperature and wind perturbations (Rayleigh friction and Newtonian cooling) toward a prescribed, zonally uniform basic state. This was achieved by removing topography and water vapor from the model and locking the wavenumber zero (zonal mean) values of divergence, vorticity, temperature, and surface pressure to their initial values throughout each model run. Thus, the model is nonlinear with respect to the magnitude of the applied heating, but no interaction is allowed between the zonally asymmetric response and the mean flow, or between the model circulation and the heating. Various studies have found that the nonlinear interactions between forced waves and the mean state are relatively small in the Tropics (Nigam 1994; Hoskins and Rodwell 1995; Jin and Hoskins 1995).

We performed experiments using both a resting, horizontally uniform basic state with a static stability in the troposphere equal to the Tropics-wide average, and basic states composed of the zonally averaged winds, temperatures, and surface pressures from the monthly mean National Centers for Environmental Prediction (NCEP) reanalysis fields corresponding to the same time periods as the TRMM PR observations used to derive the latent heating distributions. It is assumed that the specified zonal-mean climates include the dynamical influence of the zonal-mean component of tropical heating. The frictional damping coefficient applied to zonal and meridional wind perturbations from the basic state decreases linearly from $(2.5 \text{ days})^{-1}$ at the surface to a constant value of $(15 \text{ days})^{-1}$ at 800 hPa and above. The Newtonian cooling uses the same damping profile as the Rayleigh friction below 200 mb, but above this level the cooling coefficient increases linearly back up to $(2.5 \text{ days})^{-1}$ at the top of the model. The stronger damping near the surface is intended to roughly account for the effects of surface drag and vertical mixing in the boundary layer, while the larger thermal damping coefficients aloft help limit the growth of waves in the stratosphere. The CCM3 dynamical core also includes harmonic (∇^2) diffusion in the top three model levels to absorb vertically propagating planetary wave energy and weak biharmonic (∇^4) horizontal diffusion at all levels to control small-scale noise. A limited number of experiments performed with different damping parameters, horizontal diffusion coefficients, and vertical resolutions suggest that our results are not very sensitive to these aspects of the model.

The model typically reaches an equilibrium solution in about 2 weeks for experiments performed using a resting basic state. In the experiments performed using realistic basic states, baroclinic instabilities begin to distort the numerical solution in the Tropics after 15–20 days. Jin and Hoskins (1995) and Hoskins and Rodwell (1995) performed experiments with a similar model and found that the tropical and midlatitude responses are normally established in about a week, and the high-latitude pattern is established in another week. Therefore, we use day 14 averages to represent the steady-state, zonally asymmetric response to the imposed heating in all of our experiments.

5. Annual-mean experiments

In order to verify that our model produces a reasonable dynamical response to horizontal variations in tropical heating, and also provide a simple context for demonstrating how variations in stratiform rain fraction influence the response, we performed several experiments using a resting basic state and the latent heating derived from the PR annually averaged precipitation from 1998–2000 and geographically uniform stratiform rain fractions of 0%, 40%, and 70%. The column-integrated heating is the same for all three runs, so the differences between the model responses to these three heating distributions arise solely from the differences in the vertical heating structures depicted in Fig. 3b.

Figure 5a shows the 400-hPa latent heating distribution and the resulting 250-hPa streamfunction anomalies obtained using the annual mean latent heating with 0% stratiform rain fraction everywhere. Anticyclonic circulation anomalies are present over southern Asia and the Indian Ocean, while cyclonic gyres dominate the Pacific basin. This quadrapole pattern is similar to the pattern obtained for an isolated divergence anomaly near the equator (Gill 1980), and is consistent with the interpretation that intense heating over the western Pacific warm pool drives large-scale divergence anomalies and vorticity generation aloft that dominate the mean horizontal circulation in the upper tropical troposphere. The smaller streamfunction anomalies present in the Atlantic

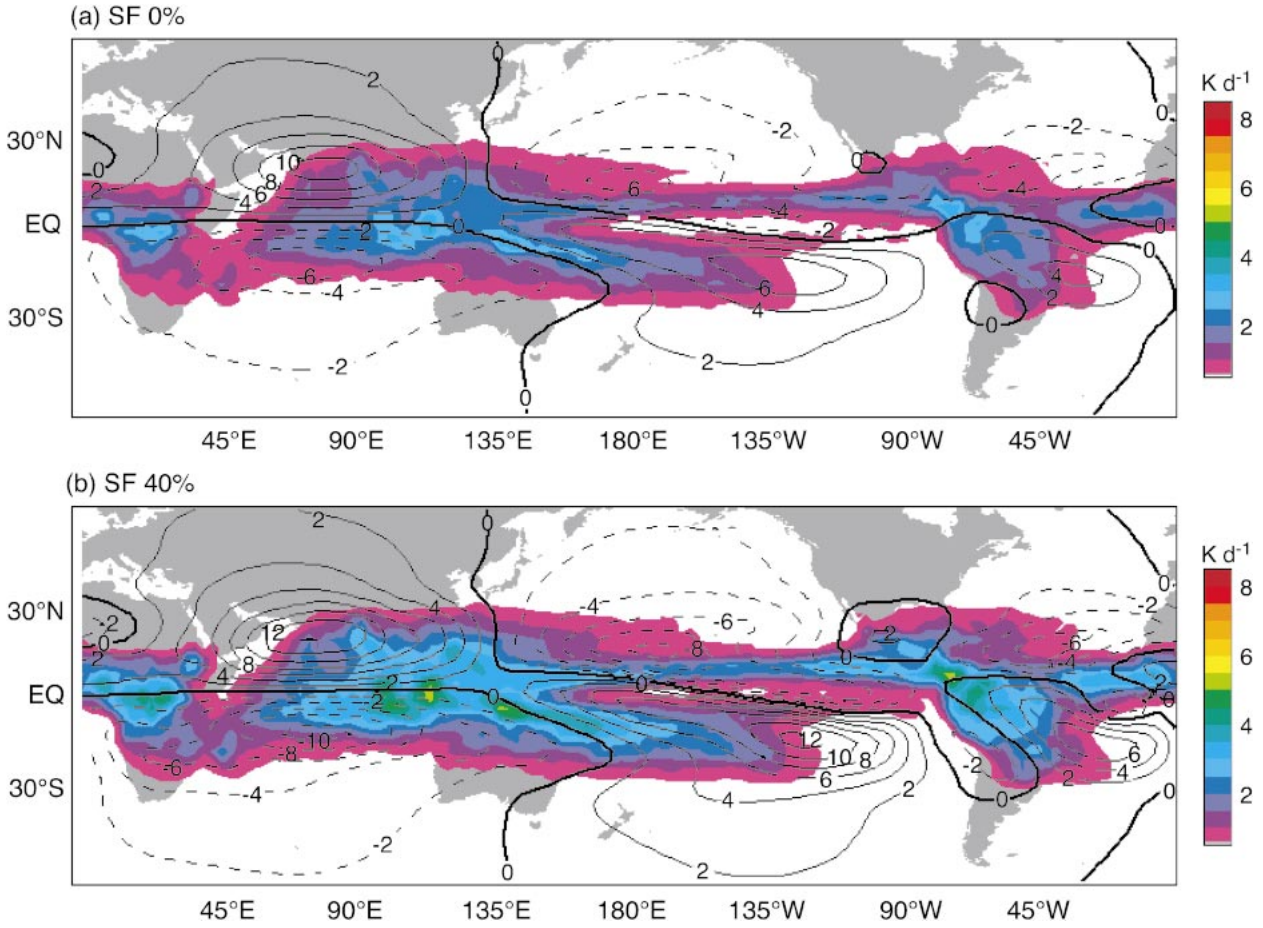

FIG. 5. The 400-hPa latent heating (shaded) and the resulting 250-hPa streamfunction anomalies (contours) for the resting basic state and latent heating derived from the PR annually averaged precipitation field and geographically uniform stratiform rain fractions of (a) 0% and (b) 40%. The streamfunction contour interval is 2×10^6 m^2 s^{-1}, and negative contours are dashed.

region reflect both local heating and the remote influence of the heating in the western Pacific. The Tropics-wide pattern bears a strong resemblance to the horizontal circulation patterns obtained by previous authors (e.g., Hartmann et al. 1984; Nigam 1994; Wang and Ting 1999), which suggests that our approach yields a reasonable large-scale response.

Figure 5b illustrates the 400-hPa latent heating and 250-hPa streamfunction response obtained when the uniform stratiform rain fraction is increased to 40%. The streamfunction and latent heating patterns in Fig. 5b are similar to those obtained in Fig. 5a, although both the midtropospheric latent heating field and the upper-level anticyclonic and cyclonic circulation features are substantially stronger in the uniform 40% case. This intensification is consistent with the increase in the vertical gradient of latent heating in the upper troposphere noted in Fig. 3b, since the generation of potential vorticity is directly proportional to the local vertical heating gradient (Haynes and McIntyre 1987).

Figures 6a–c show vertical cross sections of the zonal wind and vertical pressure velocity (ω) anomaly fields near the equator (8.5°N–8.5°S) for the integrations performed using the latent heating derived from geographically uniform stratiform rain fractions of 0%, 40%, and 70%. In Fig. 6a (the 0% case), negative ω anomalies occur over regions with large rain accumulations (i.e., equatorial Africa, the Maritime Continent and western Pacific warm pool, and Central America and the Amazon basin) and positive ω anomalies occur over regions with lower rain accumulations (i.e., the western Indian Ocean, the central and eastern Pacific, and the eastern Atlantic). The ω anomalies have maximum amplitude between 500–600 hPa, which is where the deep convective heating is strongest. The zonal wind anomaly pattern has four cells in a square wave pattern that corresponds with the flow implied by the upper-level streamfunction anomalies in Fig. 5a.

In Fig. 6b, the geographically uniform stratiform rain fraction is increased to 40% (as in Fig. 5b). The strength of the ω anomalies increases and the centers rise in altitude to 400–500 hPa in accordance with the elevation and concentration of the vertical heating profile. The centers of the zonal wind anomalies are also slightly

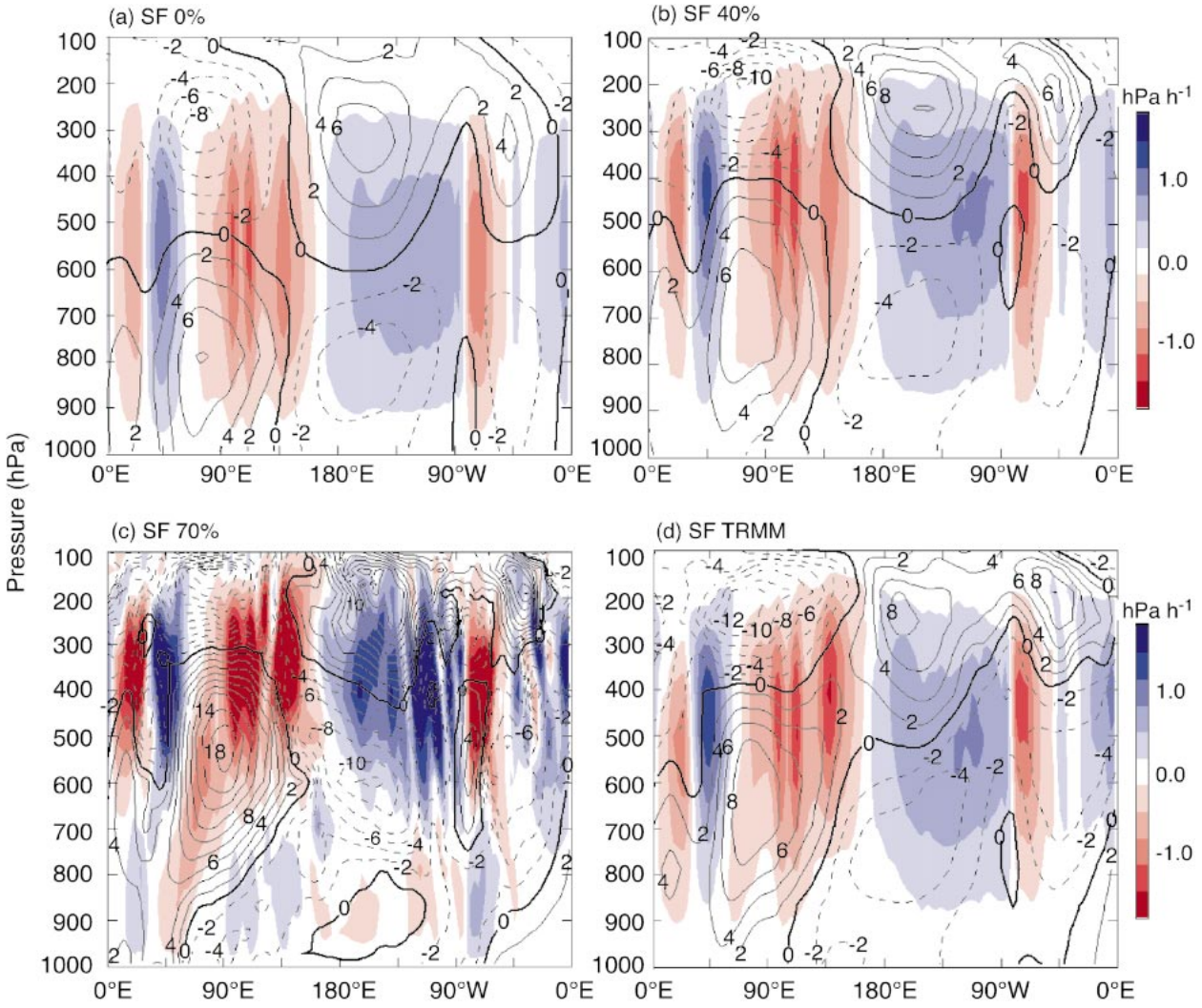

FIG. 6. Vertical cross sections of ω (shaded) and zonal wind (contours) anomaly fields averaged along the equator from 8.5°N–8.5°S for a resting basic state and latent heating derived from the PR annually averaged precipitation and stratiform rain fractions of (a) 0%, (b) 40%, (c) 70%, and (d) observed. The units for the zonal wind contours are m s^{-1}, and negative contours (easterlies) are dashed.

higher and more intense than those in the 0% case. In Fig. 6c, the latent heating based on a uniform 70% stratiform rain fraction produces the strongest response, with the highest maxima and minima centered at 350 hPa. A weaker layer of low-level ω anomalies is centered at 850 hPa, opposite in sign to the upper-level response, which reflects heating anomalies of opposite sign seen in Fig. 3b. The zonal wind anomalies are also more intense and elevated than those in the previous two scenarios. In addition, a third layer of zonal wind anomalies begins to emerge near the surface. This unusual feature is a result of the extreme assumption of a horizontally uniform 70% stratiform rain fraction.

The assumption of a geographically uniform stratiform rain fraction in the above model simulations is equivalent to assuming that there is no horizontal variation in the vertical structure of latent heating across the Tropics. This lack of horizontal variation leads to idealized circulation centers at constant heights. However, as seen in Fig. 2, stratiform rain fraction varies substantially across the Tropics. Figure 6d shows the vertical cross section of the equatorial response to the annual mean latent heating calculated using PR stratiform rain fractions from 1998–2000. The model response is most similar to the uniform 40% case, which is reasonable since the annually averaged stratiform rain fraction is ~40%. However, the circulation centers exhibit larger horizontal variations in height and vertical extent than the uniform 40% case. For example, the ω anomaly maxima and minima range in height between 400–600 hPa and the upper-level zonal wind anomaly maxima and minima are located between 200–300 hPa. Variation in the heights and vertical extents of the ω anomalies leads to a tilt in the zonal wind field. In par-

ticular, the zonal gradient in stratiform rain fraction from ~30% over Indonesia to ~60% over the eastern tropical Pacific produces vertical variations in latent heating that are associated with a tilted structure in the equatorial circulation.

Hartmann et al. (1984) assumed a heating profile for an idealized mature cloud cluster that closely resembles the profile when the stratiform rain fraction is equal to 70% (Fig. 3b). They found that the mature cloud cluster heating profile forced a more realistic Walker cell response than a purely convective profile, in part, because it produced a westward tilt with height of the simulated zonal mass flux. While the latent heating based on a uniform stratiform rain fraction of 70% produces some variation in the heights of the midlevel circulation centers (Fig. 6c), comparison with Fig. 6d suggests that a tilted zonal circulation is better simulated with a latent heating field based on the observed horizontal variation in stratiform rain fraction.

6. Seasonal cycle

In order to see if the TRMM-derived latent heating estimates can be used to produce seasonal variations in the zonally asymmetric circulation, the model was integrated using the NCEP basic states and PR precipitation and stratiform rain fractions for both June–July–August (JJA) and December–January–February (DJF) of 1998–2000. Figures 7a and 7b show the resulting 250-hPa streamfunction anomalies for JJA and DJF, respectively. In JJA, the cyclonic streamfunction anomalies over South Asia and the Indian Ocean are centered at 70°E, the anticyclonic Pacific gyre north of the equator is centered just west of the date line, the Atlantic gyre north of the equator is centered at 60°W, and the Pacific gyre south of the equator has an elongated center that spans from the date line to 90°W. There is also some evidence of wave propagation into the extratropical Southern Hemisphere in the Pacific sector.

In DJF, the main region of upper-level heating has shifted east to over the western Pacific warm pool (150°E). The streamfunction anomalies north of the equator have also shifted eastward, while the anticyclonic gyre over the Indian Ocean has weakened and split into multiple centers over southern Africa and Australia. In addition, the elongated cyclonic gyre south of the equator has separated into alternating cyclonic–anticyclonic–cyclonic streamfunction anomalies over the Pacific, South America, and the Atlantic. There is also some indication of enhanced wave propagation into the Northern (winter) Hemisphere, with only weak zonal asymmetries in the Southern (summer) Hemisphere, which is consistent with the enhanced wave propagation into the winter hemisphere noted by Jin and Hoskins (1995).

Figures 7c and 7d illustrate the NCEP reanalysis 250-hPa streamfunction field with the zonal mean removed for JJA and DJF, respectively. Between 30°N–30°S, the JJA and DJF upper-level streamfunction anomaly patterns from the TRMM-derived latent heating (Figs. 7a and 7b) show a strong qualitative agreement with the NCEP reanalysis for the same time periods, which indicates that our model captures the fundamental response of the tropical circulation to seasonal variations in the three-dimensional distribution of latent heating. However, the circulation anomalies in our model are consistently smaller in amplitude than the zonal asymmetries in the NCEP reanalysis, especially outside of 30°N–30°S.

The weak extratropical response in our model is consistent with the results of Valdes and Hoskins (1989), Wang and Ting (1999), and Held et al. (2002), who found that tropical diabatic heating forces only a weak extratropical response, and that orography, extratropical diabatic heating, transients, and wave–mean-flow interactions (none of which is present in our model) all play an important role in maintaining the observed extratropical stationary wave pattern. The smaller amplitude of the tropical circulation features in our model, relative to the zonal asymmetries in the NCEP reanalysis, is also probably associated with the lack of orography and the absence of other sources of tropical diabatic heating from our model (e.g., cloud radiative forcing), although our results are similar in magnitude to the response Held et al. (2002) obtained during the residual diabatic heating derived from NCEP reanalysis. It should be noted that neither our results nor NCEP's reanalysis fields are strictly observational and hence there is no truth involved in the comparison, only consistency. We will return to this magnitude issue in section 8.

7. El Niño

The 1998 El Niño event and the 1999 La Niña event exhibited dramatic differences in PR stratiform rain fraction and precipitation (Schumacher and Houze 2003a). In order to compare the model response to this interannual difference, another set of experiments was performed using the NCEP basic states and the PR precipitation and stratiform rain fractions for January–April 1998 (El Niño) and January–April 1999 (La Niña).

Figure 8 shows the 400-hPa latent heating distribution and the resulting 250-hPa streamfunction zonal deviations for the two events. The upper-level streamfunction response to the TRMM-derived latent heating for the 4-month La Niña season of 1999 (Fig. 8a) is similar to the DJF pattern (Fig. 7b). During La Niña, the subtropical gyres centered over the western Pacific and the couplet over the Atlantic are in the same location as in the DJF climatology, although the Pacific gyres are slightly stronger than during an average year and the Atlantic gyres are slightly weaker. Wave propagation is also enhanced into the Northern Hemisphere extratropics during the 1999 La Niña.

The TRMM-derived latent heating and upper-level streamfunction response for the 4-month El Niño season

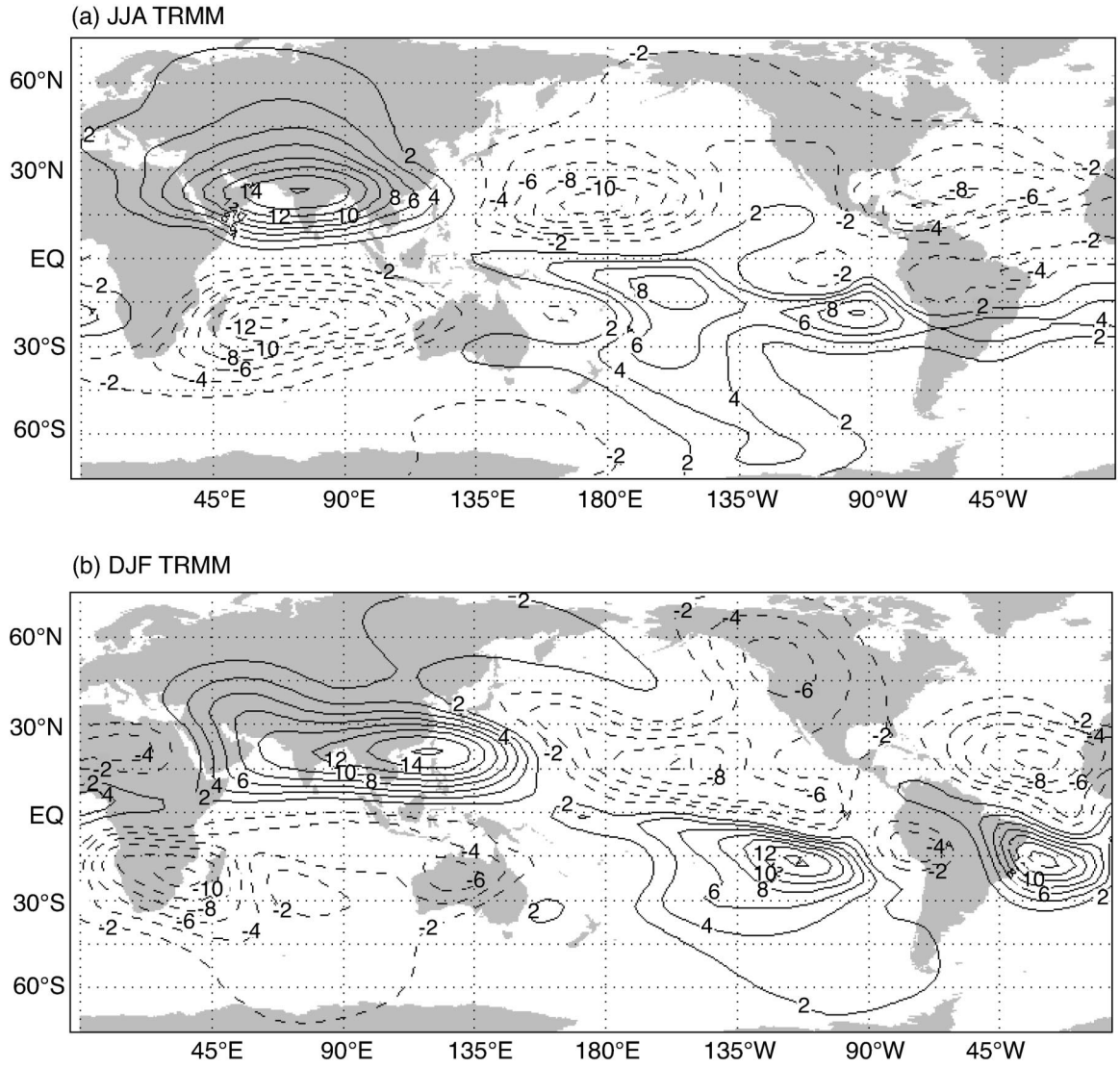

FIG. 7. The 250-hPa streamfunction anomalies for the NCEP seasonal basic-state and latent heating derived from the PR seasonally averaged precipitation and stratiform rain fraction fields for (a) JJA and (b) DJF. The streamfunction contour interval is 2×10^6 m^2 s^{-1} and negative contours are dashed. NCEP eddy streamfunctions for (c) JJA and (d) DJF. The NCEP streamfunction contour interval is 3×10^6 m^2 s^{-1}.

of 1998 (Fig. 8b) is quite different than the response for the La Niña season of 1999. During the 1998 El Niño, the precipitation field (indicated by the latent heating at 400 hPa) shifts into the central and eastern Pacific, and stratiform rain fractions get as low as 20% over Indonesia and reach almost 70% in the eastern Pacific. The longitudinally averaged precipitation is almost constant across the entire tropical band centered just south of the equator; the variations in upper-level heating are due to the dramatic west–east gradient in stratiform rain fraction. Nigam et al. (2000) show that the European Centre for Medium-Range Weather Forecasts (ECMWF) reanalysis captures some of the large-scale (i.e., stratiform) precipitation increase in the central and eastern Pacific during El Niño; however, the signal is not nearly as strong as that observed by the PR in 1998.

The major changes in the precipitation and stratiform rain fraction during the 1998 El Niño lead to significant changes in the model circulations over the Pacific. The anticyclonic gyre over southeastern Asia weakens and elongates to cover the entire Pacific basin, replacing the cyclonic gyre north of the equator in the central Pacific. The anticyclonic gyre over the Indian Ocean also elongates across the Pacific and weakens, although this change is not as pronounced as the changes in the Northern Hemisphere. The zonal deviations of the circulation in the Atlantic sector remain relatively unchanged, although the small anticyclones normally present over the western half of South America are absent.

To highlight the importance of the horizontal variation of the stratiform rain fraction during El Niño, Fig. 9 depicts vertical cross sections of the zonal wind and

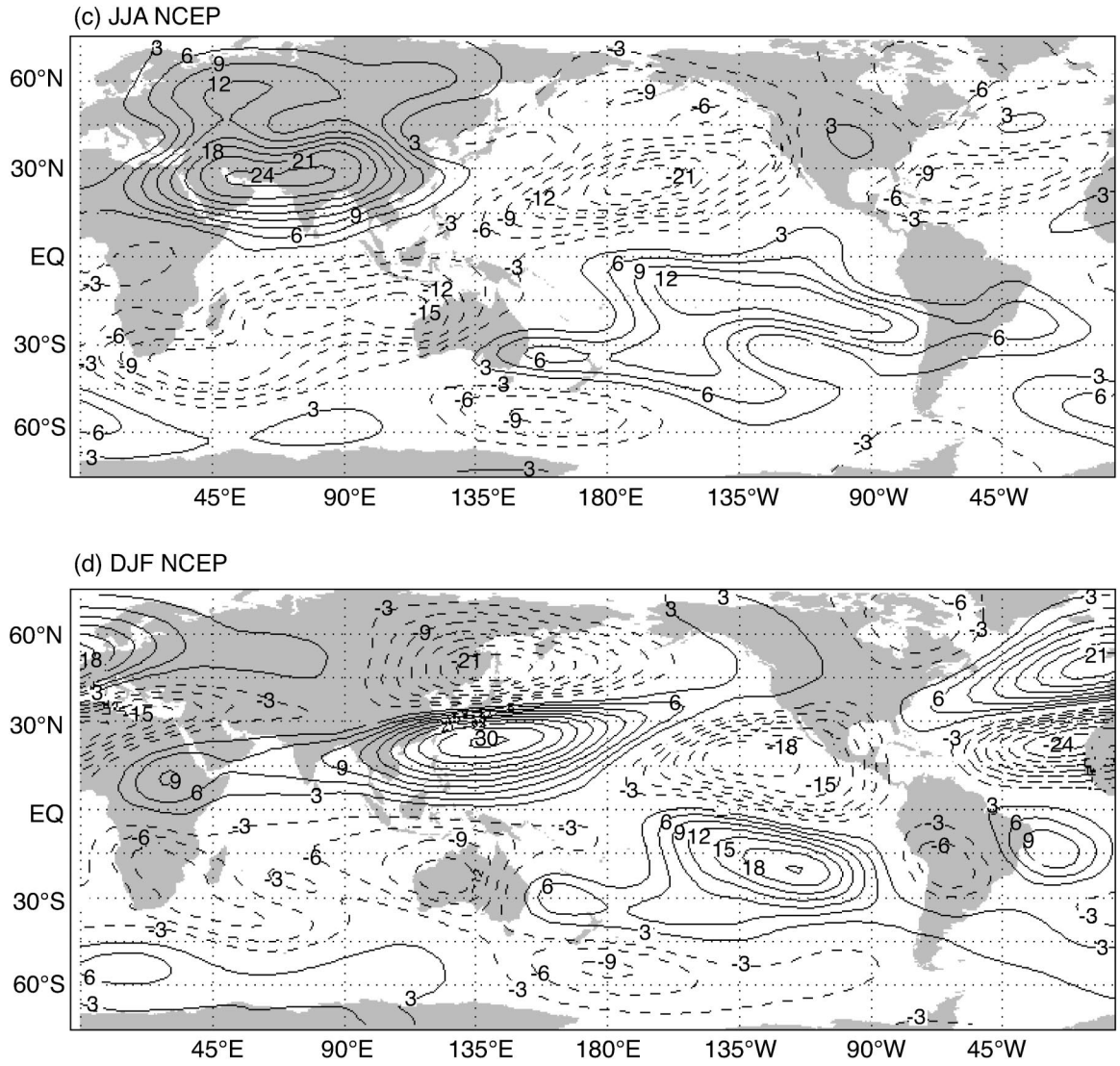

FIG. 7. (*Continued.*)

responses averaged along the equator from 8.5°N–8.5°S obtained using latent heating derived from the PR precipitation during the 1998 El Niño and geographically uniform stratiform rain fractions of 40% and 70%, along with the PR stratiform rain fraction. The model response to the latent heating based on a uniform stratiform rain fraction of 40% (Fig. 9a) is weak. Comparison with the more idealized uniform 40% model simulation in section 5 (Fig. 6b) shows that circulation centers are at similar altitudes in both model runs but are weaker during El Niño. In addition, the main region of upward motion has shifted to the central and eastern Pacific, and the four square wave pattern in the zonal wind field over the Indian Ocean and central Pacific has disappeared. When the stratiform rain fraction is increased to 70% (Fig. 9b), the circulation centers move upward and strengthen and another layer of ω and zonal wind anomalies appears at lower levels, similar to what occurred in the uniform 70% case (Fig. 6c) in section 5.

While the Tropics-wide average stratiform rain fraction increases only slightly during El Niño (to ~45%), the model response to the latent heating based on the PR stratiform rain fraction (Fig. 9c) is somewhat different than the response to the uniform 40% case (Fig. 9a). The strength of ω and zonal wind response and the presence of an additional circulation layer at lower levels is more similar to the uniform 70% case; however, negative and positive ω anomalies in Figs. 9b and 9c are not always collocated (e.g., over 90°E), and much of the height variation in circulation centers is still lacking in the uniform 70% model run. The structure and tilt in the equatorial cross section appears to be driven by the trans-Pacific gradient in stratiform rain fraction, which is especially pronounced during El Niño.

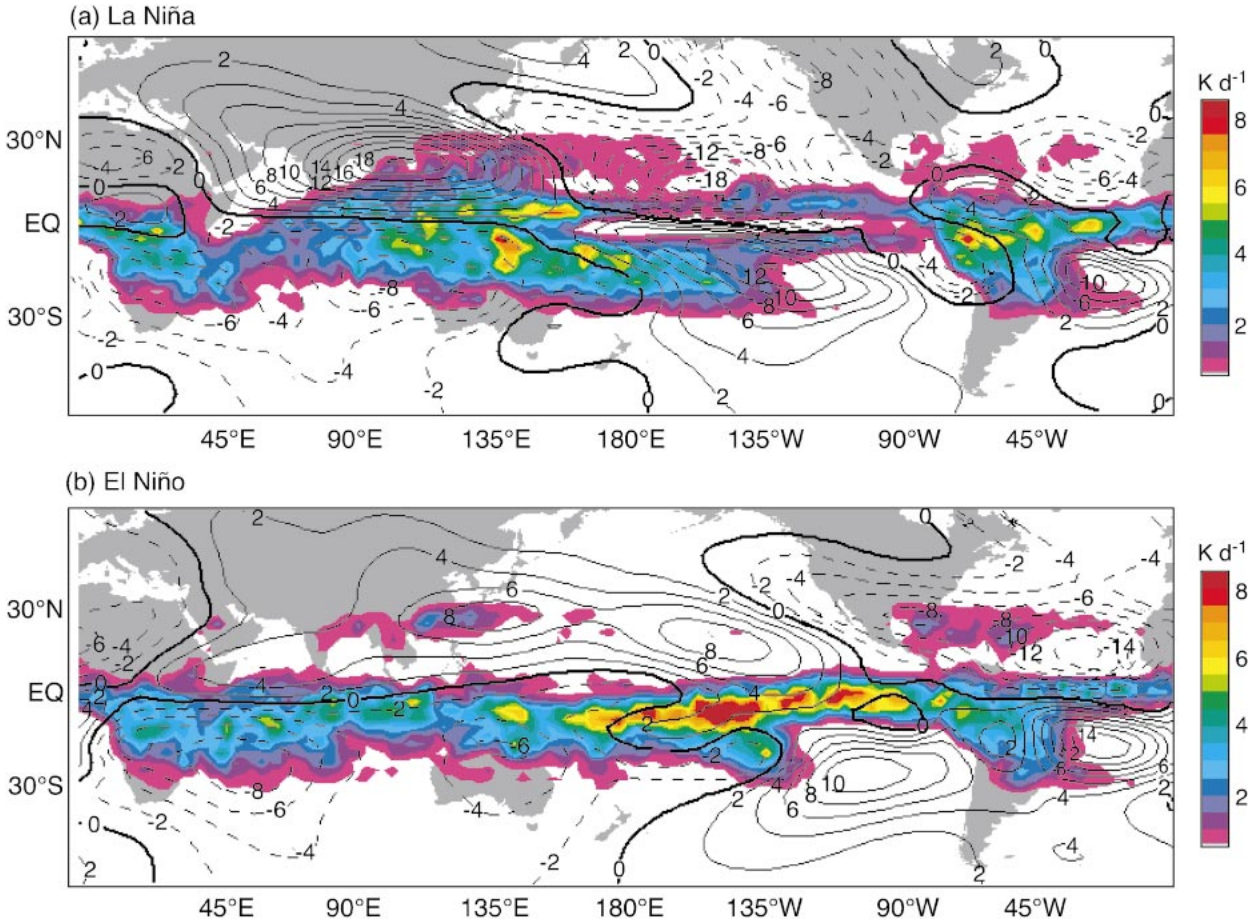

FIG. 8. The 400-hPa latent heating (shaded) and the resulting 250-hPa streamfunction anomalies (contours) for the NCEP basic state for (a) La Niña (JFMA 1999) and (b) El Niño (JFMA 1998) and latent heating derived from the PR precipitation and stratiform rain fraction fields for the same periods. The streamfunction contour interval is 2×10^6 m^2 s^{-1}, and negative contours are dashed.

8. Effects of nonprecipitating convection and cloud radiative forcing

While the crux of this paper lies in the qualitative circulation forced by the latent heating derived from Tropics-wide observations from the TRMM satellite, we would like to address possible factors that may affect both the magnitude and pattern of the model response, including the relatively strong damping and latitudinal tapering of precipitation required to keep our model stable; the absence of orography, transients, and wave–mean-flow interactions from our model; the possible underestimation of low-level precipitation by the TRMM PR; and the absence of other components of the full diabatic forcing. Valdes and Hoskins (1989) and Ting and Sardeshmukh (1993) found that using solely tropical heating and applying large changes in model damping produces only small effects in the tropical circulation, and sensitivity tests performed using untapered precipitation fields and different damping parameters indicate that these aspects of our model are not responsible for the large changes in amplitude within the Tropics. The results of previous studies (Wang and Ting 1999; Held et al. 2002) also suggest that the absence of orography, transients, and wave–mean-flow interactions are unlikely to have a strong influence on tropical circulation anomalies (except for orographic influences near the Tibetan Plateau). Bowman et al. (2003) and Serra and McPhaden (2003) found that the TRMM PR underestimates surface rain compared to buoy observations in the tropical Pacific. Sensitivity tests show that the change in the model response is, to first order, linearly related to the amplitude change in the forcing. Thus, an increase in precipitation of 20% would increase the circulation response by about 20%, but will not change the pattern of the response. Inclusion of other components of the diabatic heating field will be the focus of the rest of this section.

In the Tropics, cloud radiative forcing (CRF) represents the largest contribution to the total diabatic heating after latent heating and can account for a significant portion of the atmospheric response to tropical precipitating systems (Bergman and Hendon 2000). Also, the redistribution of latent heating by nonprecipitating convective clouds can alter the vertical gradient of the latent

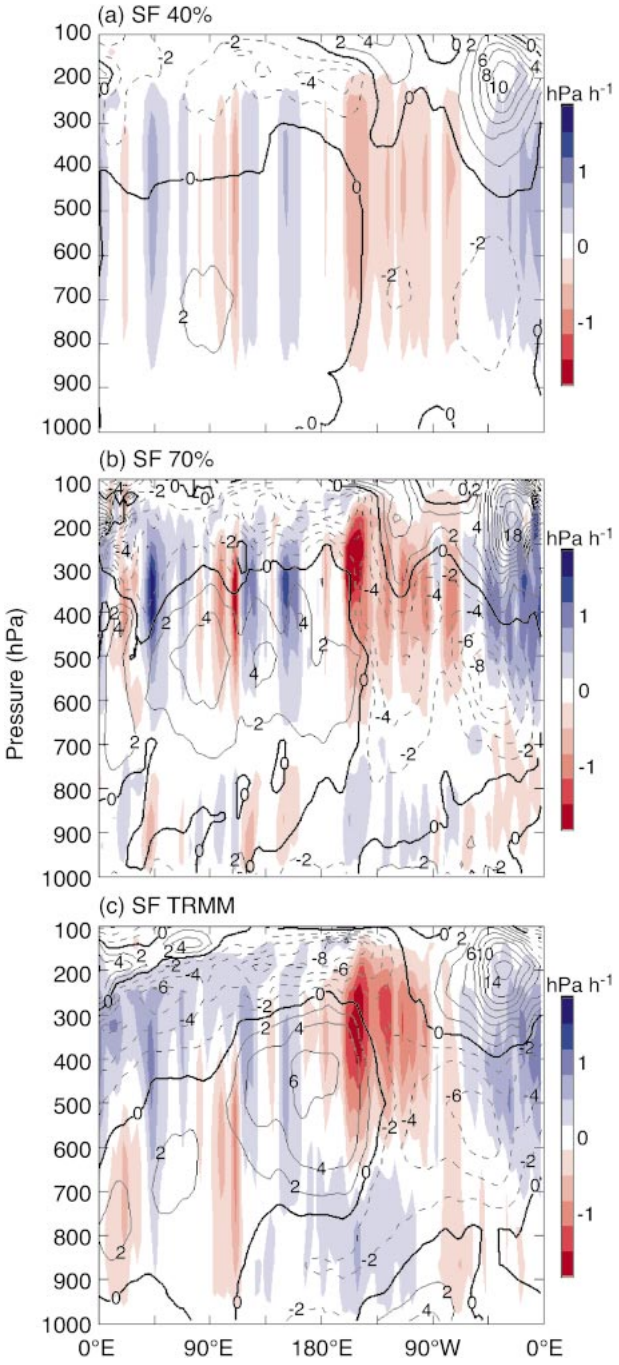

FIG. 9. Vertical cross sections of ω (shaded) and zonal wind (contours) anomaly fields averaged along the equator from 8.5°N–8.5°S for the NCEP basic state for El Niño (JFMA 1998) and latent heating derived from the PR-observed precipitation and stratiform rain fractions of (a) 40%, (b) 70%, and (c) observed. The units for the zonal wind contours are m s^{-1}; negative contours (easterlies) are dashed.

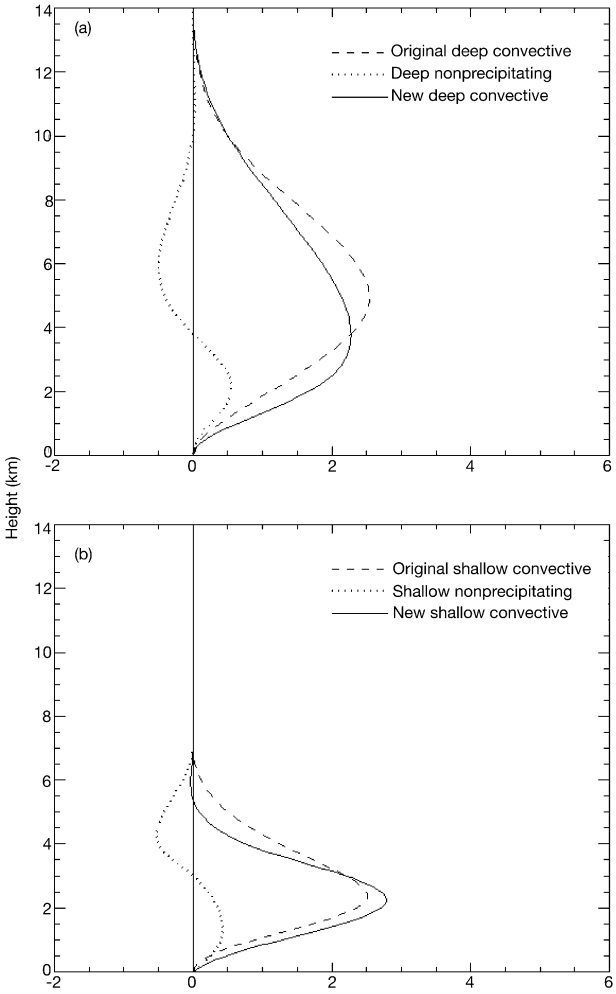

FIG. 10. Idealized latent heating profiles for nonprecipitating cumulus (dotted) in (a) deep and (b) shallow convective rain. The original convective latent heating profiles from Fig. 3a are shown (dashed) along the resulting convective latent heating profiles after the redistribution of latent heating from nonprecipitating cumulus is taken into account (solid). The x axis is meant to be nondimensional; however, it could be thought of as K day^{-1} for a specified surface rain amount.

heating profile, especially at lower levels. Simple assumptions with the PR data make the examination of CRF and nonprecipitating convection within regions of tropical precipitating systems possible.

Nonprecipitating clouds do not add latent heat to the atmosphere, although they do affect the distribution of heating in the vertical (e.g., Nitta and Esbensen 1974; Johnson and Lin 1997). The latent heating profile of a nonprecipitating cumulus cloud is positive in the lower part of the cloud, due to net positive condensation, and negative in the upper part of the cloud where detrainment occurs and evaporation exceeds condensation. Johnson et al. (1999) point out that low-level cumulus associated with the trade inversion and midlevel cumulus congestus in the vicinity of the 0°C level are prominent cloud types in the Tropics. We assume that populations of nonprecipitating cumulus and cumulus congestus occur in the same time and space domains as the precipitating clouds seen by the PR.

The dotted profiles in Fig. 10 are our assumed latent heating profiles for deep and shallow nonprecipitating

convective clouds and were constructed to be consistent with the budget studies of Nitta and Esbensen (1974) and Johnson and Lin (1997). The vertical integral of each curve is zero, so latent heat is not added to the system: each profile simply redistributes latent heating in the vertical. When the deep nonprecipitating convective profile is added to the original deep convective profile (Fig. 10a, dashed curve; see also Fig. 3a), the resulting lowering of the peak heating to 3.5 km (solid curve) is within the range of maximum heating heights seen in budget studies of deep convection (e.g., Johnson 1984). It is difficult to make an equivalent comparison in the shallow convective case (Fig. 10b) because the literature lacks budget studies that single out a shallow precipitating regime. The new convective latent heating profiles are substituted for the original convective profiles in order to calculate the four-dimensional latent heating field taking into account nonprecipitating cumulus.

Clouds associated with mature precipitating convective systems are largely opaque to infrared (IR) radiation and act to counter the IR energy loss to space that occurs under clear-sky conditions (Gray and Jacobsen 1977). Infrared CRF in mature precipitating convective systems generally warms the troposphere, except for large IR losses (cooling) near cloud top. Deep cloud systems also absorb solar radiation in their upper levels. Over a day's time, IR cooling and shortwave warming at the cloud top largely cancel one another such that CRF only weakly cools at the uppermost levels of deeper cloud systems. Houze (1982) included the radiative heating as part of the total heating profile of a tropical mesoscale system and showed that the CRF in stratiform regions acts to reinforce the upper-level latent heating maximum. Bergman and Hendon (2000) also found that CRF reinforces the circulation from latent heat release in deep convective systems, and they showed that the radiative component of shallow clouds tends to be dominated by reflection of solar radiation such that the CRF is negative.

Unlike latent heating, radiative heating is associated with the area covered by cloud rather than with the amount of rain produced. Therefore, to estimate a CRF in each rainy area, we use the TRMM PR measurement of the area covered by precipitation. For the relevant time period, each 2.5° grid box in the Tropics has a fractional area covered by shallow convective, deep convective, and stratiform radar echo as seen by the PR. However, since the cloudy area generally greatly exceeds the rainy area, we must apply some factor to the TRMM PR observed rain area to estimate the cloud cover. We refer to the International Satellite Cloud Climatology Project (ISCCP) results (Rossow and Schiffer 1991, see online at http://isccp.giss.nasa.gov) for a climatology of fractional cloud cover.[3] The fractional area covered by PR precipitation ranges from 5%–10% in regions of large rain accumulation and 1%–5% in regions of low rain accumulation, whereas the ISCCP climatology indicates cloud fractions of 60%–90% in heavy rain regions and 20%–50% in light rain regions. So as a rough estimate of fractional cloud cover associated with the PR echoes, we multiply the fractional areas covered by shallow convective, deep convective, and stratiform precipitation seen by the PR by 10 to estimate the cloud cover in each category. However, the total fractional cloud cover is never allowed to exceed 90%.

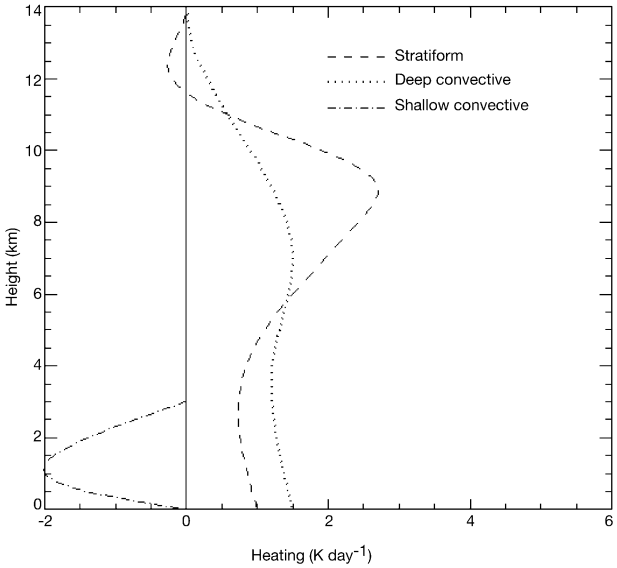

FIG. 11. Idealized cloud radiative forcing profiles in regions with shallow convective, deep convective, and stratiform rain, assuming 100% cloud cover.

Figure 11 shows the idealized CRF profiles that we apply to the area covered by each type of precipitating cloud category. The dotted curve is the CRF that applies if 100% of the area of the grid box is covered by deep convective cloud. This curve is essentially a direct cancellation of the clear-sky cooling based on Gray and Jacobson (1977). Similarly, the dashed curve shows the CRF that applies if 100% of the area of the grid box is covered by stratiform cloud. Stratiform cloud is assumed to have a base at or above the 0°C level so more warming occurs at upper levels, and less at lower levels (Webster and Stephens 1980). The shallow convective CRF (dashed–dotted) has a negative CRF in the lower troposphere (Bergman and Hendon 1998). Note that stratus decks are excluded from this exercise since we have no proxy for stratus cloud distributions using PR observations. The net radiative forcing for the grid box is obtained by multiplying each curve by the actual percentage coverage by the respective cloud type and summing to obtain the net forcing. The net CRF computed in this manner is then added to the net latent heating profile field.

[3] ISCCP cloud detection is based on variations of visible and infrared radiation from clear-sky conditions as observed by a suite of operational satellites. The cloud detection algorithm is described in Rossow and Garder (1993).

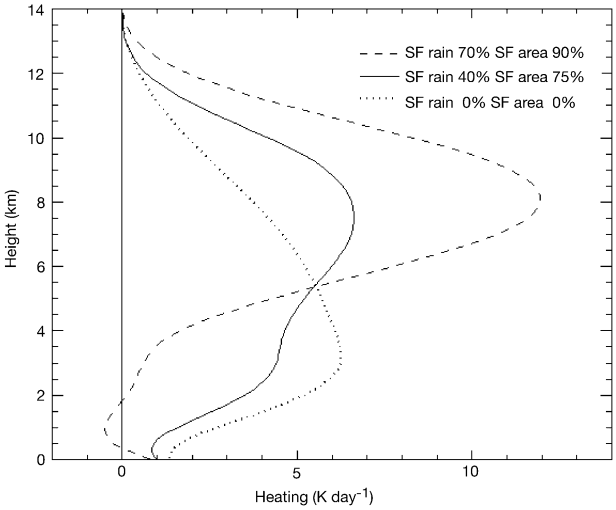

FIG. 12. Profiles of total heating (including nonprecipitating convection and CRF) for 0%, 40%, and 70% stratiform rain fraction and 0%, 75%, and 90% stratiform rain area fraction assuming 3.6 m yr^{-1} rain accumulation, 90% cloud cover, and 10% of the rain and rain area is shallow convective.

Figure 12 presents three profiles of net latent plus cloud radiative heating computed from combinations of stratiform rain fraction (for the latent heating) and stratiform rain area fraction (for the CRF) for 3.6 m yr^{-1} of rain and 90% cloud cover. Comparison to Fig. 3b shows that the additional heating profiles both increase the magnitude of the heating and alter the vertical gradient of the heating. With the additional heating, the purely convective case has a lower, stronger heating maximum at 3 km. In the case of 40% stratiform rain fraction and 75% stratiform rain area fraction, the upper-level heating maximum strengthens and is elevated to 8 km, and there is a weaker lower-level maximum at 3 km. In the case of 70% stratiform rain fraction and 90% stratiform rain area fraction, the maximum around 8 km has sharpened and there is almost no low-level cooling.

The model was run using the NCEP basic state and the heating derived from precipitation only and from precipitation with the additional heating components for DJF 1998–2000. The vertical cross sections of zonal wind and ω anomalies averaged along the equator from 8.5°N–8.5°S are shown in Fig. 13. The response to the precipitation-only latent heating (Fig. 13a) has structure similar to the model response to the annual heating and a resting basic state (Fig. 6d). The maxima and minima of ω are centered between 400–600 hPa, and a quadrapole structure of zonal wind anomalies is over the Indian Ocean and the central Pacific along with a smaller couplet over the Atlantic. The low-level zonal wind maxima and minima range from 600–800 hPa, while the upper-level zonal wind minima and maxima are around 200 hPa.

The response to the addition of the heating from nonprecipitating convective clouds and CRF is shown in Fig. 13b. The ω anomalies strengthen and extend to lower levels. The upper-level zonal wind anomalies strengthen and the centers move up to ~150 mb. The lower-level zonal wind cells strengthen slightly and ex-

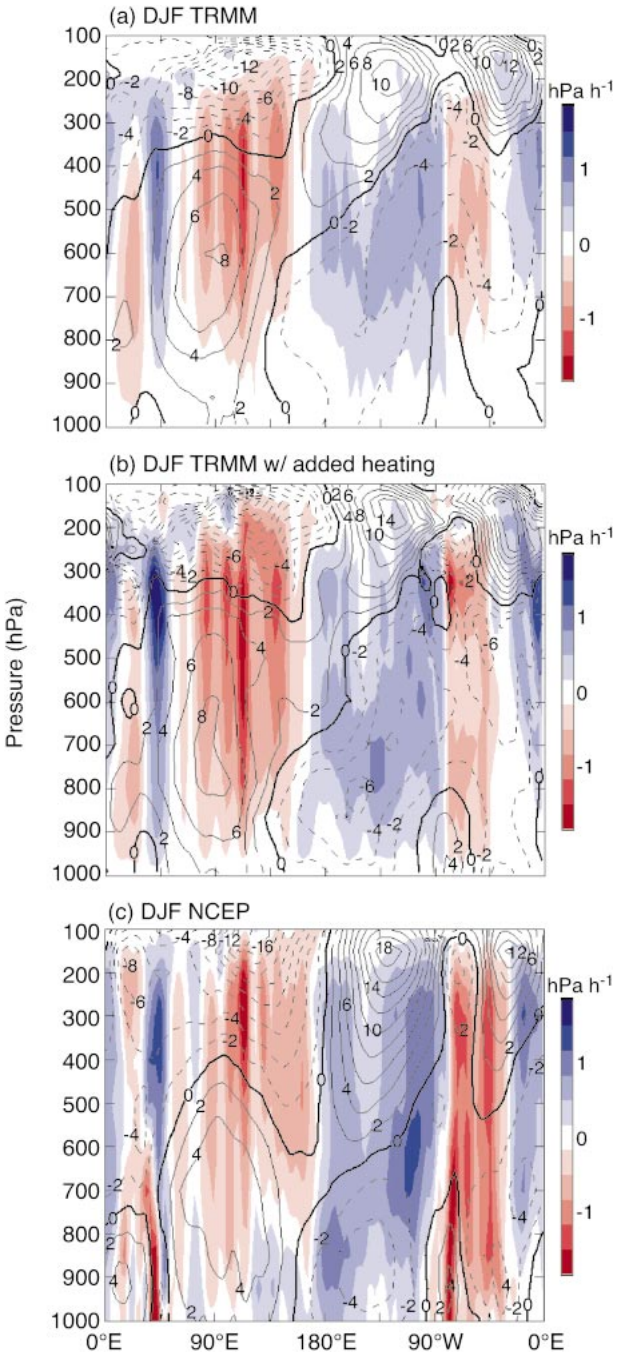

FIG. 13. Vertical cross sections of ω (shaded) and zonal wind (contours) anomaly fields averaged along the equator from 8.5°N–8.5°S for (a) model results based on PR DJF precipitation and stratiform rain fraction, (b) model results based on the PR DJF precipitation and stratiform rain fraction with additional heating from nonprecipitating convection and cloud radiative forcing, and (c) NCEP DJF reanalysis.

tend to lower levels. Despite the lack of land–sea contrasts, topography, and stratus cloud effects, the lower-level circulation response looks somewhat reasonable. Thus, the additional heating strengthens the upper-level circulation features and creates a more realistic low-level circulation, but does not change the overall structure of the pattern associated with the spatial variability in the percent of rain that is stratiform. Figure 13c shows that the response to the additional heating is more consistent with NCEP.

9. Conclusions

Observations from the TRMM PR between 1998–2000 provide the rainfall pattern across the Tropics and indicate significant geographical and temporal variability in the proportion of rain that is stratiform across the equatorial regions, most prominently across the Pacific basin (Schumacher and Houze 2003a). We have inferred the vertical distribution of heating from the stratiform rain fractions observed by the TRMM PR, in accordance with previous studies of tropical convection. The derived vertical distribution of heating varies horizontally across the Tropics in direct correspondence to the stratiform rain fraction. We have forced an idealized general circulation model with the three-dimensional latent heating derived from TRMM PR observations for different subsets of the 1998–2000 study period (i.e., seasonal and annual averages) in order to obtain the quasi-steady state, nonlinear, zonally asymmetric dynamical response. This study shows that the geographical and temporal variability in stratiform rain fraction plays an important role in shaping the structure of the large-scale tropical circulation response to precipitating cloud systems.

Simple experiments were performed using a resting basic state and the latent heating derived from annually averaged precipitation observed by the PR assuming uniform stratiform rain fractions of 0% (purely convective) and 40% (the Tropics-wide average). The model response to these latent heating distributions shows that higher stratiform rain fractions lead to elevated circulation centers and a stronger upper-level response, in agreement with Houze (1982) and Hartmann et al. (1984). However, vertical cross sections along the equator show circulations at constant heights. Recalculation of the input latent heating with the PR stratiform rain fraction leads to a model response in which the height and vertical extent of the circulation centers vary and the equatorial zonal wind field exhibits a tilted structure. The zonal gradient in stratiform rain fraction, especially the pronounced increase from ~30% over Indonesia to ~60% over the eastern tropical Pacific, is the primary reason for this horizontal variation in the height of circulation centers. If the stratiform rain fraction is assumed to be a uniform 70%, the model response shows some variation in the heights of the midlevel circulation centers, but an unrealistic circulation at lower levels results. Thus, height variations in the tropical circulation leading to a tilt in the zonal wind anomaly field are better simulated with the latent heating based on the observed, geographically varying stratiform rain fraction field than by applying a geographically uniform stratiform component.

More realistic experiments performed using NCEP basic states and PR precipitation and stratiform rain fractions from JJA and DJF show realistic seasonal variations of the upper-level streamfunction anomaly field in the Tropics. This result is in agreement with Wang and Ting (1999), who showed that diabatic heating maintains the tropical stationary waves throughout the seasonal cycle. Outside of 30°N–30°S, the upper-level wave propagation is weak. The model was forced only with a tropical heat source so we did not expect to capture the full extratropical wave train. In addition, orography, transient eddies, and nonlinear interactions between forced waves and the mean flow were not present in the model.

The response of the tropical circulation to latent heating during the 1998 El Niño is extremely sensitive to the magnitude and horizontal variability of the stratiform rain fraction. During El Niño, higher rain accumulations shift into the central and eastern Pacific. The east–west gradient in stratiform rain fraction intensifies, with stratiform rain fractions as low as 20% over Indonesia and as high as 70% in the east Pacific. These differences lead to major changes in the tropical latent heating field and greatly alter the Pacific upper-level streamfunction anomaly pattern produced by the model. The circulation response to the latent heating based on the observed stratiform rain fraction during the 1998 El Niño is stronger than the response to the latent heating based on a uniform value of 40% (the annually averaged Tropics-wide average). Latent heating based on a uniform stratiform rain fraction of 70% produced circulation anomalies closer in amplitude to the response obtained using the latent heating based on the observed El Niño stratiform rain fractions, but the uniform horizontal profile failed to capture the height variation in the ω anomalies and the tilted structure in the zonal wind field. Again, the tilt in the equatorial cross section appears to come from the spatial variability of the percent of rain that is stratiform, while the magnitude of the stratiform rain fraction dictates the strength of the upper-level circulation response.

We examined other components of the total heating profile associated with tropical precipitating systems that were not included in the precipitation-based latent heating estimates, namely, the redistribution of latent heating by nonprecipitating cumulus and cloud radiative forcing. These modifications to the heating profiles increase the magnitude of the model response and create a more realistic low-level circulation, but do not generally change the overall pattern originally forced by the spatial variability of the percent of rain that is stratiform.

This study stresses the importance of accurately capturing the stratiform rain field because the attendant variations in the latent heating structure are important to tropical and extratropical circulation variations. General circulation models have difficulty in accurately producing the stratiform component of tropical mesoscale systems (cf. PR observations with White and Saha 1995 and Nigam et al. 2000; see also Lin et al. 2004); however, efforts are being made to improve model parameterizations of the mesoscale components of deep convection (Donner et al. 2001; Fowler and Randall 2002). TRMM PR observations are useful both as targets for refinement of general circulation model physical parameterizations and tools with which to understand tropical and extratropical atmospheric circulation variability.

Acknowledgments. We thank Richard Johnson, Paul Ciesielski, and Qiang Fu for their suggestions regarding the heating profiles used in this study. We also thank Dennis Hartmann for his advice and comments. Three anonymous reviewers provided insightful comments that helped strengthen this paper. Candace Gudmundson edited the manuscript and Kay Dewar and Jill Campbell refined the figures. This research was supported by the following grants: NASA NAG5-9668, the Earth System Science fellowship NGT5-30378, NSF ATM-9873691, and the University of Washington JISAO Cooperative Agreement NA67RJ0155 (PACS).

REFERENCES

Awaka, J., T. Iguchi, H. Kumagai, and K. Okamoto, 1997: Rain type classification algorithm for the TRMM precipitation radar. *Proc. IEEE 1997 Int. Geoscience and Remote Sensing Symp.,* Singapore, IEEE, 1633–1635.

Bergman, J. W., and H. H. Hendon, 1998: Calculating monthly radiative fluxes and heating rates from monthly cloud observations. *J. Atmos. Sci.,* **55,** 3471–3491.

——, and ——, 2000: Cloud radiative forcing of the low-latitude tropospheric circulation: Linear calculations. *J. Atmos. Sci.,* **57,** 2225–2245.

Bowman, K. P., A. B. Phillips, and G. R. North, 2003: Comparison of TRMM rainfall retrievals with rain gauge data from the TAO/TRITON buoy array. *Geophys. Res. Lett.,* **30,** 1757, doi:10.1029/2003GL017552.

Chiang, J. C. H., S. E. Zebiak, and M. A. Cane, 2001: Relative roles of elevated heating and surface temperature gradients in driving anomalous surface winds over tropical oceans. *J. Atmos. Sci.,* **58,** 1371–1394.

Cifelli, R., and S. A. Rutledge, 1998: Vertical motion, diabatic heating, and rainfall characteristics in north Australia convective systems. *Quart. J. Roy. Meteor. Soc.,* **124,** 1133–1162.

DeMaria, M., 1985: Linear response of a stratified tropical atmosphere to convective forcing. *J. Atmos. Sci.,* **42,** 1944–1959.

Donner, L. J., C. J. Seman, R. S. Hemler, and S. Fan, 2001: A cumulus parameterization including mass fluxes, convective vertical velocities, and mesoscale effects: Thermodynamic and hydrological aspects in a general circulation model. *J. Climate,* **14,** 3444–3463.

Fowler, L. D., and D. A. Randall, 2002: Interactions between cloud microphysics and cumulus convection in a general circulation model. *J. Atmos. Sci.,* **59,** 3074–3098.

Frank, W. M., and J. L. McBride, 1989: The vertical distribution of heating in AMEX and GATE cloud clusters. *J. Atmos. Sci.,* **46,** 3464–3478.

Geisler, J. E., 1981: A linear model of the Walker cell. *J. Atmos. Sci.,* **38,** 1390–1400.

Gill, A. E., 1980: Some simple solutions for heat-induced tropical circulation. *Quart. J. Roy. Meteor. Soc.,* **106,** 447–462.

Gray, W. M., and R. W. Jacobson Jr., 1977: Diurnal variation of deep cumulus convection. *Mon. Wea. Rev.,* **105,** 1171–1188.

Hartmann, D. L., H. H. Hendon, and R. A. Houze Jr., 1984: Some implications of the mesoscale circulations in tropical cloud clusters for large-scale dynamics and climate. *J. Atmos. Sci.,* **41,** 113–121.

Haynes, P. H., and M. E. McIntyre, 1987: On the evolution of vorticity and potential vorticity in the presence of diabatic heating and frictional or other forces. *J. Atmos. Sci.,* **44,** 828–841.

Held, I. M., M. Ting, and H. Wang, 2002: Northern winter stationary waves: Theory and modeling. *J. Climate,* **15,** 2125–2144.

Hoskins, B. J., and M. J. Rodwell, 1995: A model of the Asian summer monsoon. Part I: The global scale. *J. Atmos. Sci.,* **52,** 1329–1340.

Houze, R. A., Jr., 1982: Cloud clusters and large-scale vertical motions in the tropics. *J. Meteor. Soc. Japan,* **60,** 396–410.

——, 1989: Observed structure of mesoscale convective systems and implications for large-scale heating. *Quart. J. Roy. Meteor. Soc.,* **115,** 425–461.

——, 1993: *Cloud Dynamics.* Academic Press, 573 pp.

——, 1997: Stratiform precipitation in regions of convection: A meteorological paradox? *Bull. Amer. Meteor. Soc.,* **78,** 2179–2196.

Iguchi, T., T. Kozu, R. Meneghini, J. Awaka, and K. Okamoto, 2000: Rain-profiling algorithm for the TRMM precipitation radar. *J. Appl. Meteor.,* **39,** 2038–2052.

Jin, F., and B. J. Hoskins, 1995: The direct response to tropical heating in a baroclinic atmosphere. *J. Atmos. Sci.,* **52,** 307–319.

Johnson, R. H., 1984: Partitioning tropical heat and moisture budgets into cumulus and mesoscale components: Implications for cumulus parameterization. *Mon. Wea. Rev.,* **112,** 1590–1601.

——, and X. Lin, 1997: Episodic tradewind regimes over the western Pacific warm pool. *J. Atmos. Sci.,* **54,** 2020–2034.

——, T. M. Rickenbach, S. A. Rutledge, P. E. Ciesielski, and W. H. Schubert, 1999: Trimodal characteristics of tropical convection. *J. Climate,* **12,** 2397–2418.

Kiehl, J. T., J. J. Hack, G. B. Bonan, B. A. Boville, D. L. Williamson, and P. J. Rasch, 1998: The National Center for Atmospheric Research Community Climate Model: CCM3. *J. Climate,* **11,** 1131–1149.

Kistler, R., and Coauthors, 2001: The NCEP–NCAR 50-year reanalysis: Monthly means CD-ROM and documentation. *Bull. Amer. Meteor. Soc.,* **82,** 247–267.

Kozu, T., and Coauthors, 2001: Development of precipitation radar onboard the Tropical Rainfall Measuring Mission (TRMM) satellite. *IEEE Trans. Geosci. Remote Sens.,* **39,** 102–116.

Kummerow, C., W. Barnes, T. Kozu, J. Shiue, and J. Simpson, 1998: The Tropical Rainfall Measuring Mission (TRMM) sensor package. *J. Atmos. Oceanic Technol.,* **15,** 809–817.

Lin, J., B. Mapes, M. Zhang, and M. Newman, 2004: Stratiform precipitation, vertical heating profiles, and the Madden–Julian Oscillation. *J. Atmos. Sci.,* **61,** 296–309.

Mapes, B. E., and R. A. Houze Jr., 1995: Diabatic divergence profiles in western Pacific mesoscale convective systems. *J. Atmos. Sci.,* **52,** 1807–1828.

Newman, M., P. D. Sardeshmukh, and J. W. Bergman, 2000: An assessment of the NCEP, NASA, and ECMWF reanalyses over the tropical west Pacific warm pool. *Bull. Amer. Meteor. Soc.,* **81,** 41–48.

Nigam, S., 1994: On the dynamical basis for the Asian summer monsoon rainfall–El Niño relationship. *J. Climate,* **7,** 1750–1771.

——, C. Chung, and E. DeWeaver, 2000: ENSO diabatic heating in ECMWF and NCEP–NCAR reanalyses, and NCAR CCM3 simulation. *J. Climate,* **13,** 3152–3171.

Nitta, T., and S. Esbensen, 1974: Heat and moisture budget analyses using BOMEX data. *Mon. Wea. Rev.,* **102,** 17–28.

Olson, W. S., C. D. Kummerow, Y. Hong, and W. K. Tao, 1999: Atmospheric latent heating distributions in the Tropics derived from satellite passive microwave radiometer measurements. *J. Appl. Meteor.,* **38,** 633–664.

Rossow, W. B., and R. A. Schiffer, 1991: ISCCP cloud data products. *Bull. Amer. Meteor. Soc.,* **72,** 2–20.

——, and L. C. Garder, 1993: Cloud detection using satellite measurements of infrared and visible radiances for ISCCP. *J. Climate,* **6,** 2341–2369.

Schumacher, C., and R. A. Houze Jr., 2003a: Stratiform rain in the Tropics as seen by the TRMM precipitation radar. *J. Climate,* **16,** 1739–1756.

——, and ——, 2003b: The TRMM precipitation radar's view of shallow, isolated rain. *J. Appl. Meteor.,* **42,** 1519–1524.

Serra, Y. L., and M. J. McPhaden, 2003: Multiple time- and space-scale comparisons of ATLAS buoy rain gauge measurements with TRMM satellite precipitation measurements. *J. Appl. Meteor.,* **42,** 1045–1059.

Simpson, J., R. F. Adler, and G. R. North, 1988: Proposed Tropical Rainfall Measuring Mission (TRMM) satellite. *Bull. Amer. Meteor. Soc.,* **69,** 278–295.

Steiner, M., R. A. Houze Jr., and S. E. Yuter, 1995: Climatological characterization of three-dimensional storm structure from operational radar and rain gauge data. *J. Appl. Meteor.,* **34,** 1978–2007.

Sui, C.-H., and K.-M. Lau, 1989: Origin of low-frequency (intraseasonal) oscillations in the tropical atmosphere. Part II: Structure and propagation of mobile wave-CISK modes and their modification by lower boundary forcings. *J. Atmos. Sci.,* **46,** 37–56.

Tao, W. K., J. Simpson, S. Lang, M. McCumber, R. Adler, and R. Penc, 1990: An algorithm to estimate the heating budget from vertical hydrometeor profiles. *J. Appl. Meteor.,* **29,** 1232–1244.

——, and Coauthors, 2001: Retrieved vertical profiles of latent heat release using TRMM rainfall products for February 1998. *J. Appl. Meteor.,* **40,** 957–982.

Thompson, R. M., Jr., S. W. Payne, E. E. Recker, and R. J. Reed, 1979: Structure and properties of synoptic-scale wave disturbances in the intertropical convergence zone of the eastern Atlantic. *J. Atmos. Sci.,* **36,** 53–72.

Ting, M., and P. D. Sardeshmukh, 1993: Factors determining the extratropical response to equatorial diabatic heating anomalies. *J. Atmos. Sci.,* **50,** 907–918.

Valdes, P. J., and B. J. Hoskins, 1989: Linear stationary wave simulation of the time-mean climatological flow. *J. Atmos. Sci.,* **46,** 2509–2527.

Waliser, D. E., A. Shi, J. R. Lanzante, and A. H. Oort, 1999: The Hadley circulation: Assessing NCEP/NCAR reanalysis and sparse in-situ estimates. *Climate Dyn.,* **15,** 719–735.

Wang, H., and M. Ting, 1999: Seasonal cycle of the climatological stationary waves in the NCEP–NCAR reanalysis. *J. Atmos. Sci.,* **56,** 3892–3919.

Webster, P. J., and G. L. Stephens, 1980: Tropical upper-tropospheric extended clouds: Inferences from winter MONEX. *J. Atmos. Sci.,* **37,** 1521–1541.

White, G., and S. Saha, 1995: Three-dimensional diabatic heating fields from the NCEP/NCAR reanalysis. *Proc. 20th Climate Diagnostics Workshop,* Seattle, WA, U.S. Department of Commerce, 284–287.

Wu, Z., E. S. Sarachik, and D. S. Battisti, 2000: Vertical structure of convective heating and the three-dimensional structure of the forced circulation on an equatorial beta plane. *J. Atmos. Sci.,* **57,** 2169–2187.